Structural Characterization of Siliceous Spicules from Marine Sponges

Gianluca Croce,* Alberto Frache,* Marco Milanesio,* Leonardo Marchese,* Mauro Causà,* Davide Viterbo,* Alessia Barbaglia,† Vera Bolis,† Giorgio Bavestrello,‡ Carlo Cerrano,§ Umberto Benatti,¶ Marina Pozzolini,¶ Marco Giovine,‖ and Heinz Amenitsch**

*Dipartimento di Scienze e Tecnologie Avanzate, Università del Piemonte Orientale "A. Avogadro", I-15100 Alessandria, Italy; †Dipartimento di Scienze Chimiche Alimentari Farmaceutiche e Farmacologiche, Università del Piemonte Orientale "A. Avogadro", I-28100 Novara, Italy; ‡Dipartimento di Scienze del Mare, Università Politecnica delle Marche, I-60100 Ancona, Italy; §Dipartmento per lo Studio del Territorio e sue Risorse, Università di Genova, 16132 Genova, Italy; ¶Dipartmento di Medicina Sperimentale sezione Biochimica, Università di Genova, I-16132 Genova, Italy; ‖Centro Nazionale delle Ricerche, Direzione Progetto Finalizzato Biotecnologie, I-16132 Genova, Italy; and **Institute of Biophysics and X-Ray Structure Research, Austrian Academy of Sciences, A-8042 Graz, Austria

ABSTRACT Siliceous sponges, one of the few animal groups involved in a biosilicification process, deposit hydrated silica in discrete skeletal elements called spicules. A multidisciplinary analysis of the structural features of the protein axial filaments inside the spicules of a number of marine sponges, belonging to two different classes (Demospongiae and Hexactinellida), is presented, together with a preliminary analysis of the biosilicification process. The study was carried out by a unique combination of techniques: fiber diffraction using synchrotron radiation, scanning electron microscopy (SEM), thermogravimetric analysis (TGA), differential scanning calorimetric (DSC), Fourier transform infrared spectroscopy (FTIR), and molecular modeling. From a phylogenetic point of view, the main result is the structural difference between the dimension and packing of the protein units in the spicule filaments of the Demospongiae and the Hexactinellida species. Models of the protein organization in the spicule axial filaments, consistent with the various experimental evidences, are given. The three different species of demosponges analyzed have similar general structural features, but they differ in the degree of order. The structural information on the spicule axial filaments can help shed some light on the still unknown molecular mechanisms controlling biosilicification.

INTRODUCTION

The biological formation of amorphous hydrated silica, biosilicification, occurs in a wide variety of organisms (Simpson and Volcani, 1981; Voronkov et al., 1977; Bendz and Lindqvist, 1977). It should be noted that among the more general biomineralization processes (Mann, 2001) those in which silica is involved are described in a wide pattern of living beings, from single cell organisms to higher plants and animals. Research into the mechanisms controlling the process has highlighted proteins and proteoglycans as possible control molecules (Perry and Keeling-Tucker, 2000). In particular, siliceous sponges, one of the few animal groups involved in a biosilification process, deposit hydrated silica in discrete skeletal elements called spicules. Two classes of sponges produce siliceous spicules: i), Demospongiae, characterized by cellular organization and monoaxonic or tetraxonic spicules; and ii), Hexactinellida, characterized by sincitial organization and hexaradiate spicules. Two kinds of spicules are produced: megascleres, generally elongated, which compose the main architecture of the sponge skeleton, and microscleres, very variable in shape and size, with ancillary functions.

The different phases of spicule secretion have been elucidated in Demospongiae, where siliceous spicules are produced within specialized cells (sclerocytes) (Simpson, 1984) and contain an organic axial filament (Garrone, 1978), triangular in section, around which hydrated silica is periodically deposited, giving rise to a concentric arrangement. In some species axial filaments are found free in the mesohyl, and their presence has been related to an extra cellular secretion of spicules (Uriz et al., 2000; Custodio et al., 2002).

It is generally assumed that spicule growth is a bidimensional process: the increase in length is affected by the elongation of the filament, whereas the increase in width is determined by the apposition of the silica (Uriz et al., 2000).

In Demospongiae, the organic axial filament, which functions as template for silica deposition, is constituted by peculiar proteins called silicateins. Nowadays three silicateins from different sponges have been described (Shimizu et al., 1998; Krasko et al., 2000; Murakami, 2002) and all these proteins have a great similarity with cathepsin (Berti and Storer, 1995; Krasko et al., 1997). In particular, comparison between the silicatein and cathepsin L sequences shows that the six cysteine residues forming intramolecular disulfide bridges in cathepsins are conserved in silicateins, suggesting that the three-dimensional structures of the two proteins are quite similar.

The detailed molecular mechanisms of biosilica deposition in sponges, as well as the natural substrata of silicateins, are still unknown, and their study is made difficult by the complex organization of the axial filament.

The recently described silica deposition mediated by block copolypeptides (Cha et al., 2000; Morse et al., 2000; Muller

Submitted February 6, 2003, and accepted for publication September 18, 2003.

Address reprint requests to Davide Viterbo, E-mail: davide.viterbo@mfn.unipmn.it.

© 2004 by the Biophysical Society

0006-3495/04/01/526/09 $2.00

et al., 2002) represents an elegant model suggesting that complex quaternary structures should play a fundamental role in spicule shape control. Unfortunately, the rather aggressive chemical procedures of filament extraction, based on the use of HF/NH_4F (Shimizu et al., 1998), are likely to change drastically its quaternary structure. Moreover, the presence of silicateins of different molecular weight inside the filament (Uriz et al., 2000) is indicative of a complex structure involving different amounts of various proteins, some of which are insoluble. For these reasons a complete structural reconstruction of the filament using native or recombinant silicateins cannot be carried out.

The reported (Shimizu et al., 1998) preliminary x-ray diffraction analysis of axial protein filaments indicated that they are constituted by several units of silicatein α, forming a regular repeating structure of 17.2-nm periodicity. This structural characterization was however carried out on filaments extracted from the spicules by a rather strong treatment, which may cause structural changes and/or denaturation of the protein. The possibility of obtaining some structural information on the filaments inside the spicules can certainly give a more realistic picture of their organization. The main aim of this article is the structural study of the axial filament of the spicules, carried out with a unique combination of techniques: scanning electron microscopy (SEM), thermogravimetric and calorimetric analysis, infrared spectroscopy, fiber diffraction, and theoretical molecular modeling. In this study we have analyzed both mega- and microscleres of the demosponges *Geodia cydonium*, *Petrosia ficiformis*, *Tethya aurantium*, and of the hexactinellid *Scolymastra joubini* (Table 1).

MATERIALS AND METHODS

For this study the spicules of four species were used: the three demosponges *G. cydonium*, *T. aurantium*, *P. ficiformis*, and the hexactinellid *S. joubini*. Specimens of *G. cydonium* and *T. aurantium* were collected in the coastal lagoon of Porto Cesareo (Apulian Coast), those of *P. ficiformis* were collected on the rocky cliff of Portofino Promontory (Ligurian Sea), whereas those of *S. joubini* are from the Italian Antarctic Station of Terra Nova Bay (Ross Sea).

Spicules are freed from the organic matter by immersion in hydrogen peroxide (200 vol) changed each day for two weeks. They are then rinsed in distilled water and dried at 60°C. From the total bulk of spicules the macroscleres are partially removed with tweezers. The remaining material is then suspended in 100% ethanol and aspired with a Pasteur pipette previously elongated on a Bunsen. In this way, the aspired material is constituted mainly by microscleres. This procedure is then repeated three times until the complete isolation of microscleres.

The spicule morphology was analyzed by SEM on a Leica Stereoscan 420. The samples for the thermal analyses were prepared by grinding the spicules in a mortar. The thermogravimetric analysis (TGA) was carried out on a Thermal Analyst (TA) instrument (SDT2960 model) by keeping 10–15 mg sample under a constant flux of air and using a temperature ramp of 10°C/min. The differential scanning calorimetric (DSC) analysis was carried out on a Pyris 1 power-compensation calorimeter equipped with a Intracooler 2P by Perkin Elmer. To eliminate the physisorbed water, the sample (5–6 mg in an Al pan) was initially kept isothermally at 25°C (30 min) under a constant flux of N_2. Then it was heated up to 580°C by using a temperature ramp of 10°C/min (first run) and cooled down again to 25°. A second run was subsequently performed following the same procedure as for the first run. The second run curves (in which no thermal effects were detected) were assumed in all cases to be a reasonable baseline, and they were thus subtracted from the first run, to highlight the thermal effects produced during the first run. The heat absorbed by the samples, during the different processes occurring upon heating, was determined as ΔH (J/g, normalized to unit mass) by integrating the peaks using a standard Perkin Elmer program.

FTIR spectra (resolution of 4 cm^{-1}) were collected on samples shaped as thin disk pellets of ~10 mg using an ATI Mattson spectrometer equipped with a high-vacuum, variable-temperature infrared cell (LB-100 by Infraspac, Novosibirsk, Russia).

Diffraction experiments were carried out by the Austrian SAXS beamline (BL 5.2 L) (Amenitsch et al., 1998) at the ELETTRA Synchrotron Light Laboratory (Trieste, Italy), using x-rays of wavelength $\lambda = 0.1540$ nm and spicules data sets were collected with a 2D CCD-detector (diameter 115 mm; Photonic Science, Robertsbridge, UK), positioned at 872.4 mm from the sample. For the long spicules of *G. cydonium*, *T. aurantium*, and *S. joubini* the samples were either bundles of 10–15 almost parallel spicules or single spicules, depending on the type of experiment. For the smaller spicules of *P. ficiformis* the samples were a collection of randomly oriented spicules, giving rise to a powder-like diffraction pattern. The two-dimensional data analysis was performed using the FIT2D program (Hammersley, 1995; Hammersley et al., 1996).

The almost constant outcome of measurements repeated on a limited number of spicule samples for each species, also from different batches collected in different times, was convincing evidence that different individuals of the same species give reproducible results. Finally our deductions were validated by the agreement of the results obtained from different experimental techniques.

The theoretical investigation was performed employing the HYPERCHEM (Hypercube, Gainesville, FL) suite of programs for the manipulation and the molecular mechanics (MM) study of the protein. The ab initio study was carried out with the GAUSSIAN98 program (Frisch et al., 1998).

TABLE 1 Summary of the morphological features of the different spicule samples, as obtained from the SEM analysis, together with the weight loss percent determined by TGA (20–700°C interval) and the energy involved in the thermal degradation of the samples heated in the 25–580°C range, measured as ΔH (J/g) by DSC

Sponge species	Spicule type	Length (μm)	Section (μm)	Diameter (μm)	Weight loss (%)	ΔH (J/g)	T_{max} (°C)
S. joubini	Oxeas	500–2000	20–100	–	15	119	116
						584	432
G. cydonium	Oxeas	2500–3000	10–50	–	9	>436	436
G. cydonium	Sterrasters	–	–	50	–	–	–
T. aurantium	Strogyloxeas	2000–2400	17	–	10	831	472
T. aurantium	Sphaerasters	–	–	57	–	–	–
P. ficiformis	Oxeas	150–200	10	–	8	641	371

Graphic analysis and visualization of the molecular models was performed with MOLDRAW (Ugliengo et al., 1993).

RESULTS AND DISCUSSION

Scanning electron microscopy

The morphology of different kinds of spicules was analyzed by SEM with energy dispersive spectrometry (EDS) analysis, which indicated that in all samples the inorganic envelope is composed almost exclusively by Si and O. Megascleres of *S. joubini*, *G. cydonium*, and *P. ficiformis* are oxeas (elongated spicules with two sharp tips), whereas those of *T. aurantium* are strongyloxeas (elongated spicules with one sharp and one rounded tip) (Hooper and Van Soest, 2003). Their length is variable from around 200 μm in *P. ficiformis* to a few millimeters (*S. joubini*, *G. cydonium*, and *T. aurantium*). Only *T. aurantium* and *G. cydonium* show microsclere spicules with a radiate symmetry: sterrasters in *G. cydonium* and sphaerasters in *T. aurantium*. Their diameter is ~50–60 μm.

The presence of cavities in megascleres was revealed by grinding the samples. For the *P. ficiformis* sample the diameter of these cavities was estimated to be around 1 μm, in agreement with De Vos et al. (1991). These cavities are the sites where the proteins responsible for the spicule growth are hosted.

Thermal analysis

The thermal analysis measurements were carried out to monitor the presence of organic matter in the samples, and to investigate the mechanisms of their thermal decomposition at increasing temperatures, as well as the energetic involved (last two columns of Table 1).

Thermogravimetric results

Microscleres of *G. cydonium* and *T. aurantium* show no significant weight loss in the range 20–700°C, indicating that in these samples the organic matter is absent or its content is less than 1% in weight. The other spicules have a positive signal during the thermal treatment: in fact megascleres of the demosponges *G. cydonium*, *P. ficiformis*, and *T. aurantium* show a weight loss of ~10%, whereas those of the hexactinellid *S. joubini* show a weight loss of ~15%. The estimated error on the values of the weight loss is of ~1%. The relevant thermograms are shown in Fig. 1. The weight loss undergone by the samples upon heating is interpreted as due to either the elimination of water coordinated to the protein units inside the siliceous matrix or to the degradation of the organic matter itself.

The analysis of the first derivative of the thermograms shows that spicules of *S. joubini* have a faster weight loss with respect to that of the other samples (Fig. 1). This is an indication that in the Hexactinellid spicules the protein filaments may be less closely packed than in Demospongiae.

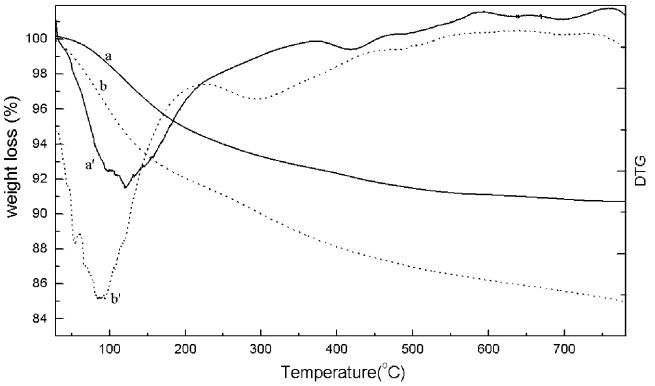

FIGURE 1 Thermogravimetric analyses, in the temperature range 20–800°C, of *T. aurantium* (*a*) and *S. joubini* (*b*) spicule samples together with their derivatives (*a′* and *b′*).

DSC calorimetric results

In Fig. 2 a selection of the DSC thermograms obtained by heating some spicule samples in the 25–580°C interval is reported. *S. joubini* (*a*), *G. cydonium* (*b*), *T. aurantium* (*c*), and *P. ficiformis* (*d*) megascleres were chosen because they show significant thermal effects upon heating. Indeed endothermic peaks were revealed for these samples, whereas no deviation from the baseline was detected for the others, i.e., sterrasters of *G. cydonium* and sphaerasters of *T. aurantium*, the thermal profiles of which were virtually identical to those obtained for commercial silicas (either amorphous or crystalline; thermograms not reported for brevity). The features of the peaks associated to the endothermic effects produced upon heating the samples were better highlighted by subtracting the second run (*dashed line*) from the first run (*thin solid line*, see the Materials and Methods section for details). This procedure

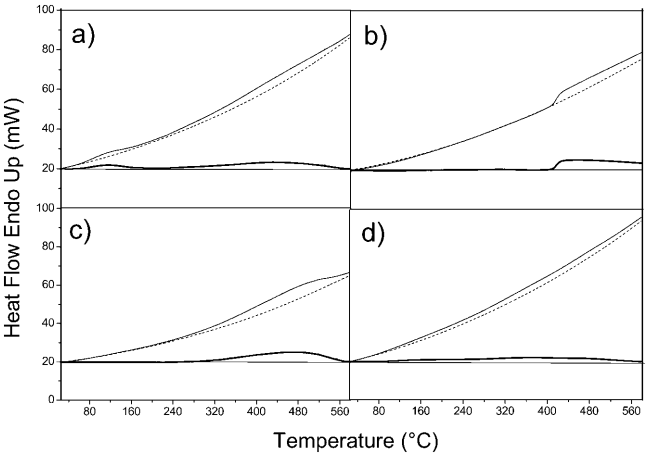

FIGURE 2 DSC traces of *S. joubini* (*a*), *G. cydonium* (*b*), *T. aurantium* (*c*), and *P. ficiformis* (*d*) spicule samples heated in the 30–580°C interval (10°C/min, under dry N_2 flow). Solid thin line, first run; dashed line, second run; thick solid line, first-second run.

appeared to be reasonable in that during the second run heating no more energy transfer was observed, indicating that the process occurred during the first run heating caused an irreversible modification of the system investigated. In the case of the microsclere samples for which no thermal effects were detected, the first and second runs' thermal profiles were hardly distinguishable.

The thermal profile obtained for the systems investigated confirmed the quantitative TGA evidence described above, i.e., not all systems undergo a significant weight loss upon heating, but only spicules containing more than 1% protein filament give a thermal response to the heating, which is caused by modifications (either structural or chemical) of the organic matter inside the silica matrix (see Table 1). The DSC traces, however, show remarkable differences between the four spicules for which thermal effects were observed. Two endothermic peaks, at low (116°C) and high (432°C) temperature were observed for oxeas of *S. joubini*, whereas only one peak at high T was observed for oxeas of *G. cydonium* and strogyloxeas of *T. aurantium* (436 and 472°C, respectively). For the oxeas of *P. ficiformis* too, only one peak was observed, but extremely broad and starting at low T (<100°C). The maximum of this peak was only approximately localized at 371°C, and could be reasonably considered as a mean value averaged over several peaks associated to different phenomena occurring at very close T-values. Also the high temperature maximum of *S. joubini* shows a similar type of broadening.

The DSC measurements were repeated up to six times to confirm the onset of the endothermic effects in the case of the various samples investigated. The estimated error on the T_{max} values is of about $\pm 1°$ and the error on ΔH, derived by integration, is $\pm 10\%$ for the sharper maxima and greater for the broader ones.

The different thermal profile shown by the various spicules may be mainly due to two different factors governing the thermal response of the systems to the heating, and namely: i), different processes actually occur in the different systems, owing to the different chemical composition of the organic matter located within the spicule cavity, and in particular owing to the protein/coordinated water ratio; and ii), the efficiency of the energy transfer from the furnace to the organic matter located within the spicule holes is dominated by the thickness of the walls of the silica matrix, which can be different according to the nature of the spicules. It is difficult on the basis of the data to discriminate between the two factors, which are possibly inextricably intermingled, but it is worth noting that the low T peak in the case of the oxeas of *S. joubini* is due to weakly energetic phenomena that likely involve either the loss of coordinated water or structural modifications in the protein filament. The former process is accompanied by weight loss (see TGA data), the latter not. As for the high T peak in the same system, it likely corresponds to the degradation of the organic matter, accompanied by a weight loss. The energetic involved during the heating of *S. joubini* is significantly larger than in the other cases, in agreement with the TGA results (see Table 1). The evidence that the overall energetic involved during the heating of *S. joubini* is significantly larger than in the other cases, whereas the onset of the low temperature process is lower, should be interpreted as due to the fact that there is a greater amount of organic matter and the biomolecules in the Hexactinellid spicules are less tightly bound.

Another factor that must be taken into account to interpret the different behavior of the various spicules is the morphology of the spicules investigated. *P. ficiformis* spicules are very thin needles (150–200 μm) with a section of only $\sim$10 μm. This means that the heat transfer from the furnace to the organic matter located in the needle cavities is probably the most efficient among the examined samples. Thus, low and high T peaks are not distinguishable as independent phenomena.

In the case of *G. cydonium* oxeas the onset temperature of the process is the highest, and the process is not fully accomplished at $T < 600$°C, indicating that either the walls of the silica matrix are extremely thick, or the biomolecules inside the cavities are particularly tightly bound.

Spectroscopic analysis

FTIR spectroscopy was employed to characterize the surface of siliceous materials, in particular to evaluate the presence of both surface hydroxyls and organic molecules, with particular interest to the spicule proteins.

The transmittance spectrum (Fig. 3) of spicules recorded at *RT* is characterized by the presence of the typical vibrational modes of silica in the 1300–500 cm^{-1} range: two bands due to the asymmetric (1200 cm^{-1}) and symmetric stretching (800 cm^{-1}) of the Si-O-Si groups, respectively. The bands in the 2200–1600 cm^{-1} range are due to overtones modes of silica (2000 cm^{-1}, 1875 cm^{-1}, and 1645 cm^{-1}) (Burneau and Gallas, 1998).

In the 3700–2400 cm^{-1} range a broad band is present, due to the stretching of –OH and –NH groups engaged in hydrogen bonds. The lower frequency side of this band is associated to the presence of protein amino acids in the sample. This is confirmed by the effects of thermal treatments in vacuum at increasing temperatures, illustrated in Fig. 3. The features of these spectra, recorded during thermal treatment, indicate the presence of different hydrogen bonds corresponding both to interactions between the different amino acids of the protein and to organic-inorganic interactions between protein and silica. Indeed, up to 100°C the thermal treatment causes a decrease of the –NH band in the 3200–2400 cm^{-1} range, due to the thermal degradation of the protein amino groups. Subsequently, from 100 to 400°C, a decrease of the –OH band in the 3700–3000 cm^{-1} range, due to the degradation of the hydroxyl groups of the amino acids, is recorded, whereas a band at 3680 cm^{-1}, attributable to the stretching modes of silanol hydroxyls of

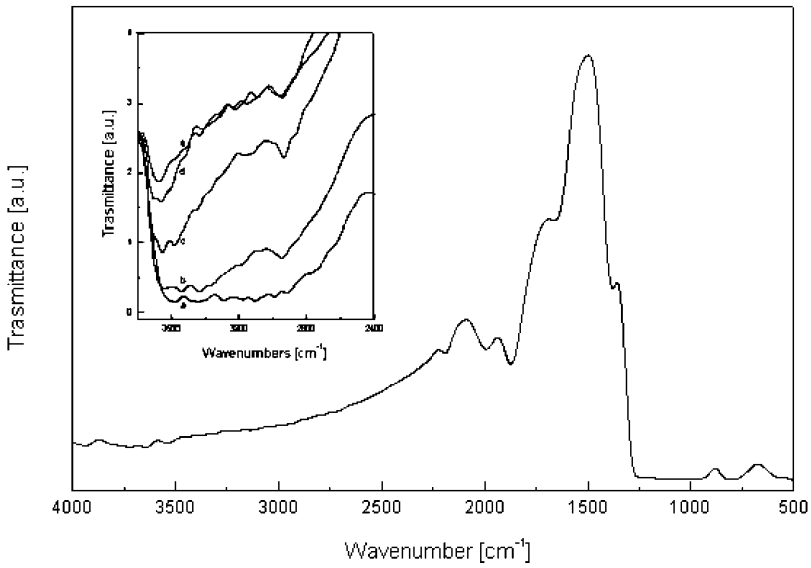

FIGURE 3 FTIR transmittance spectrum of *S. joubini* spicule sample recorded at *RT*. In the box the decrease of the broad band in the 3700–2400 cm^{-1} range during the thermal treatment in vacuum (*a*, *RT*; *b*, 100°C; *c*, 250°C; *d*, 400°C; *e*, 500°C) is shown.

the inorganic structure, becomes evident upon evacuation at 250°C (*curve c*). This feature indicates that these –OH groups at room temperature must be strongly involved in hydrogen bond interactions with the organic matter.

Fig. 4 shows the FTIR spectra of the *T. aurantium* sample in the 1800–1400 cm^{-1} range during the thermal treatments in vacuum. It is possible to observe a complex band with two main contributions at 1630 cm^{-1} and at 1660 cm^{-1}. These two modes are in the region of the C=O stretching of the peptide groups and form the so-called ''amide I bands'' (Haris and Severcan, 1999). These bands, which persist at temperatures above 100°C, provide information about the presence of protein molecules in *T. aurantium* and allow characterizing the predominant secondary structure of the polypeptide chains in the proteins (Haris and Severcan, 1999). In fact the amide I bands in the 1620–1640 cm^{-1} range of protein vibrational spectra can be attributed to β-sheet structures, whereas the infrared absorption in the range 1650–1658 cm^{-1} indicates the presence of α-helical conformations. Indeed, in *T. aurantium* silicatein (Shimizu et al., 1998) both structures are present, but the relative intensities of the bands show that the β-sheet conformations are prevailing. As already mentioned the primary amino-acid sequence of silicatein is very similar to that of Cathepsin L (Berti and Storer, 1995; Krasko et al., 1997), indicating that the three-dimensional structure of these two proteins should also be similar. Indeed an analysis of the three-dimensional structure of Cathepsin L, solved by x-ray diffraction, shows that there are 20 β-sheet structures and only 10 α-helices (Guncar et al., 1999).

Similar FTIR spectra were recorded also for *S. joubini* and *P. ficiformis* with very similar results, indicating the presence of proteins with a large percent of β-sheets in their structures.

Finally the FTIR spectra of the *G. cydonium* and *T. aurentium* microscleres only show the typical absorption bands of pure silica and confirm that these samples can not contain significant amounts of organic matter.

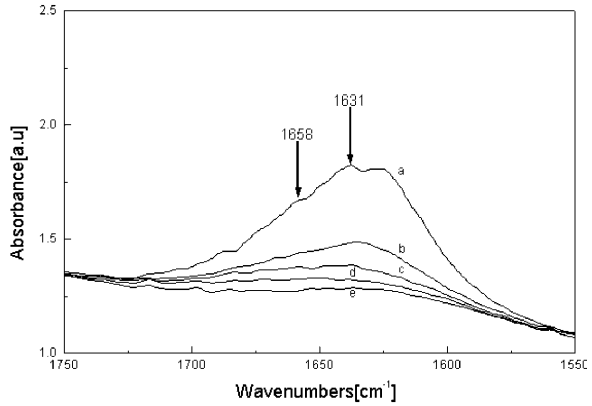

FIGURE 4 FTIR spectra of the *T. aurantium* spicule sample in the 1800–1400 cm^{-1} range during thermal treatment in vacuum (*a*, *RT*; *b*, 100°C; *c*, 250°C; *d*, 400°C; *e*, 500°C).

Fiber diffraction measurements

The aim of these fiber diffraction experiments, carried out at the SAXS beamline of the ELETTRA synchrotron radiation facility in Trieste was to obtain some structural information on the protein units inside the spicules, to achieve a more realistic picture of their organization. As indicated in Table 1, *T. aurantium*, *G. cydonium*, and *S. joubini* present spicules of sufficient length to be oriented inside a boron-glass capillary. This allowed the collection of fiber diffractograms from a still sample composed by a bundle of well-aligned (maximal estimated offset $\pm 5°$) spicules. *P. ficiformis* only gives very thin and short spicules (<200 μm), which can not be oriented by insertion in a capillary. A detailed report on the analysis of the fiber diffraction patterns of *G. cydonium*

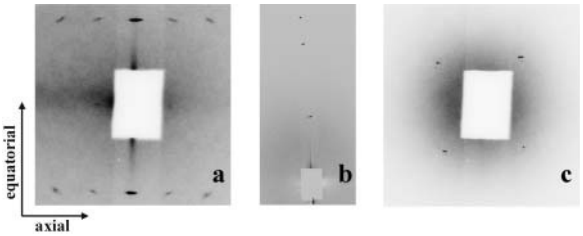

FIGURE 5 X-ray fiber diffraction patterns of *T. aurantium*. (*a*), *G. cydonium* (*b*), and *S. joubini* (*c*) spicule samples.

and *S. joubini* has been recently published (Croce et al., 2003).

The sharp spots in the diffraction patterns shown in Fig. 5 indicated that the protein units forming the central filaments inside the spicules must be organized with a very high degree of order. A summary of the measurement conditions and of the observed diffraction spacings ($S = 2\ \sin\theta/\lambda = 1/d$) is given in Table 2. The measurements were repeated between two and four times on different samples of each species with practically constant results with an estimated standard deviation of 0.002 nm^{-1}.

The protein units appear to be packed in a compact hexagonal way and from the position and distribution of the spots it is possible to derive some structural parameters. The most immediate result is the different volume occupied by the individual protein units forming the spicule filaments in samples of different origin. Indeed, from the *S*-values reported in the last column of Table 2 we could obtain a repeat ($a = d\sqrt{3}/2$) of ~5.8(1) nm for Demosponge spicules (*T. aurantium*, *G. cydonium*, and *P. ficiformis*) and of ~8.4(1) nm for the Hexactinellid one (*S. joubini*).

The different number and disposition of the diffraction spots obtained from different samples indicates that the degree of order varies from species to species. *G. cydonium* spicules show equatorial spots up to the third order (Fig. 5 *b*), which are consistent with a very regular hexagonal arrangement (Fig. 6 *a*) of protein units aligned along the spicule axis (Fig. 6 *b*). The presence of nonequatorial spots in the diffraction patterns of *T. aurantium* and *S. joubini* (Fig. 5, *a* and *c*) suggests also some degree of order along the spicule axis. For *S. joubini* a hexagonal packing of spirally oriented

TABLE 2 Summary of the fiber diffraction measurements on different types of spicules

Sponge species	Spicule shape	No. and type of reflections	Smallest $S = 1/d$ value (1/nm)
G. cydonium	Oriented oxeas	6 sharp spots	0.196 (2)
T. aurantium	Oriented strongiloxeas	>15 sharp spots	0.200 (2)
P. ficiformis	Randomly oriented oxeas	3 sharp rings	0.196 (2)
S. joubini	Oriented oxeas	4 sharp spots	0.137 (2)
T. aurantium	Sphaerasters	No diffraction	–
G. cydonium	Sterrasters	No diffraction	–

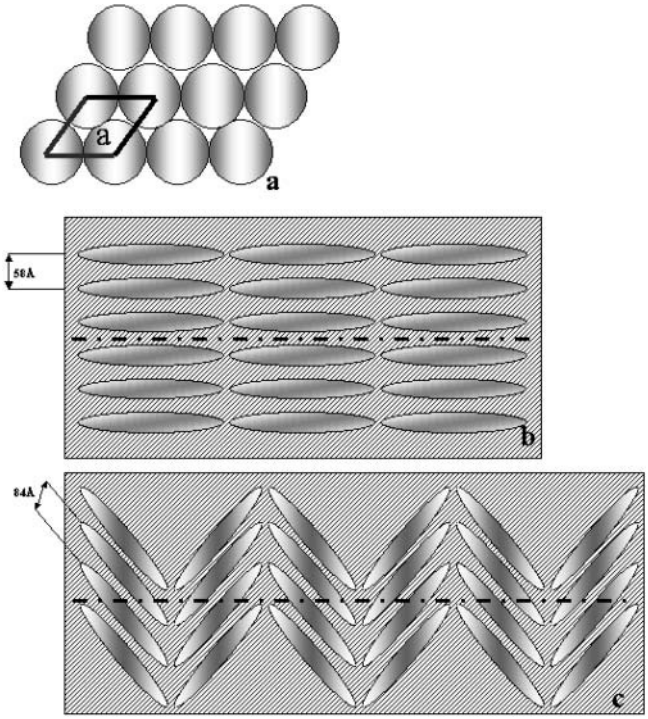

FIGURE 6 (*a*) 2D hexagonal packing; (*b*) structural model of the organization of the filaments in *G. cydonium* spicules; and (*c*) structural model of the organization of the filaments in *S. joubini* spicules. The dot and dash lines represent the longitudinal axis of the filament.

protein units elongated along the spicule axis, consistent with the 2D model of Fig. 6 *c*, can be derived (Croce et al., 2003). Inspection of Fig. 6 shows that the two different patterns of protein units in the axial filaments of spicules from different sponge families are consistent with a more dense packing in the Demosponge *G. cydonium* (*pattern b*) than in the Hexactinellid *S. joubini* (*pattern c*), in agreement with the results of our TGA and their derivatives (Fig. 1).

The diffraction spots in all our patterns are much sharper than one would normally expect from a fiber, and this feature can be explained by assuming that the silica present in the axial filament (Uriz et al., 2000) is organized around the protein units as a highly ordered mesoporous material (Croce et al., 2003; Grosso et al., 2002). The analysis and interpretation of the more complex diffraction patterns from *T. aurantium* strongiloxeas (Fig. 5 *a*) is still in progress.

Finally, the absence of diffraction signals in the experiments carried out on *T. aurantium* and *G. cydonium* microscleres confirms that probably these samples do not contain significant amounts of organized protein matter, as also suggested by the TGA, DSC, and FTIR measurements.

MOLECULAR SIMULATIONS

As we have seen, because of the high sequence homology, it is reasonable to expect that the three-dimensional structure of

silicatein is quite similar to that of cathepsin L (Berti and Storer, 1995; Krasko et al., 1997). The first step of the theoretical study was therefore the download of the crystal structure of cathepsin L (Guncar et al., 1999) from the Brookhaven Protein Database (Berman et al., 2000) (identification code 1ICF). At first the NAG ligand used for crystallization and the crystallization water molecules were removed from the structure of cathepsin L and all hydrogen atoms were added, using the computer program HYPERCHEM 6.0. A MM energy minimization, with the AMBER force field (Cornell et al., 1995), was then used to adjust the coordinates of all the atoms. The optimized cathepsin L did not vary significantly from the original crystal structure.

The so-called ''catalytic triad'' of cathepsin L is formed by residues Cys^{26}, His^{165}, and Asn^{184}, and in silicatein two of these residues, His^{165} and Asn^{184}, are conserved, whereas Cys^{26} becomes Ser^{26}.

Since it can be supposed that these amino acids might play some role in the polymerization of silica (Cha et al., 1999; Zhou et al., 1999), the next step was to build a sensible model of the active site of silicatein, by replacing the original amino acid Cys of cathepsin L with the Ser in position 26, although maintaining His^{165} and Asn^{184}. Using the same modeling conditions employed earlier, a new MM optimization of this substituted protein, called pseudosilicatein, does not reveal large changes with respect to the crystal structure and to the optimized cathepsin L. In fact the superimposition of the two optimized models shows that the protein folding does not change and the active sites present analogous interatomic distances between the residues. In particular the distance between the two α-carbons of Ser^{26} and His^{165} in pseudosilicatein remains of ~6.2 Å.

We then tried to clarify the role of Ser and His in silica biomineralization (Cha et al., 1999; Zhou et al., 1999). Indeed these two polar amino acids can interact with orthosilicic acid present in marine aqueous solutions and favor silica dimerization. Having characterized the active site of silicatein by MM calculations, this model was used as the starting point for an ab initio density functional theory (DFT) study with GAUSSIAN98 (Frisch et al., 1998).

The ab initio study was carried out on a gas-phase model of the catalytic site. The amino acids Ser^{26} and His^{165} were cut out from the structure of pseudosilicatein, saturated with hydrogen atoms, and their main chains were fixed to their MM optimized positions, although the side chains were allowed to move. This system was first refined at the HF level using the STO-3G basis set. Then the obtained structure was further optimized at the B3LYP level using the 6-31g(d,p) basis set. The final model shows that the side chains are free to rotate and able to form an hydrogen bond between the alcohol group on the C^{β} of serine and the N of the imidazole ring of histidine: the O···H distance is 1.89 Å (Fig. 7).

Subsequently we constructed two plausible models. In the first, called complex A, we introduced two molecules of silicic acid in the catalytic site depicted in Fig. 7. In the second model, called complex B, both a $Si(OH)_4$ group and a $Si(OH)_3O^-$ moiety, a possible simple product of the decomposition of organosilica compounds (Cha et al., 1999; Zhou et al., 1999), were added to the catalytic site. The two models were refined and optimized as before to determine the thermodynamic feasibility of the formation of hydrogen and covalent bonds.

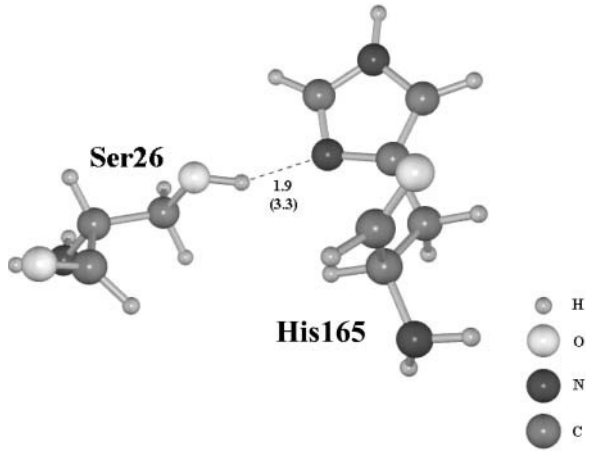

FIGURE 7 Relative positions of the Ser^{26} and His^{165} residues of the silicatein catalytic site obtained from the theoretical modeling.

Complex A turned out to be mainly stabilized by six hydrogen bonds and the binding energy (*BE*) of the adduct was $BE = E_{\text{complexA}} - (E_{\text{catalytic-site}} + 2E_{\text{Si(OH)}_4}) = -84$ kJ mol^{-1}. This model showed that the amino acids have the capability, through the rotation of their side chains, of bringing the molecules of orthosilicic acid together.

Also in complex B the rotation of the amino acid side chains can bring together the $Si(OH)_4$ and the $Si(OH)_3O^-$ groups, but this is now followed by the formation of

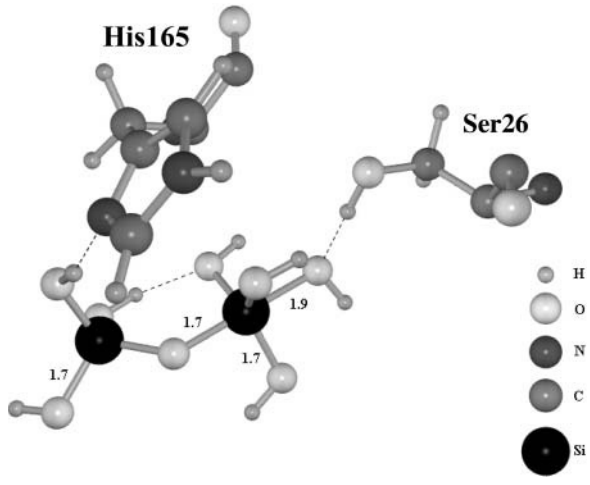

FIGURE 8 Model of complex B, representing the formation of a penta-coordinated $(OH)_3Si\text{-}O\text{-}Si(OH)_4$ species.

a pentacoordinated Si complex [$(OH)_3$Si-O-Si$(OH)_4$], depicted in Fig. 8. Indeed, the formation energy (*FE*) of complex B with respect to the reactants is rather large, i.e., $FE = E_{\text{complexB}} - (E_{\text{catalytic-site}} + E_{\text{Si(OH)}_4} + E_{\text{Si(OH)}_3\text{O}-}) = -289$ kJ mol^{-1}. Such a large *FE* highlights the dimerization of orthosilicic acid when both the neutral and the ionic forms are present. The binding energy of complex B ($BE = E_{\text{complexB}} - (E_{\text{catalytic-site}} + E_{(OH)_3\text{Si-O-Si(OH)}_4}) = -79$ kJ mol^{-1}) is comparable to that of complex A, even if only four hydrogen bonds are present. The $(OH)_3$Si-O-Si$(OH)_4$ dimer is a likely intermediate of the biomineralization of Si.

CONCLUSIONS

A general overview on the structural organization of the proteinaceous filament inside spicules is presented. A better understanding of the complex phenomenon of biosilicification should be achieved by means of a multidisciplinary approach, in which the biochemical data obtained from the studies on purified (Shimizu et al., 1998) or recombinant silicatein (Krasko et al., 2000; Cha et al., 1999; Zhou et al., 1999) are integrated with the results obtained from the structural analysis of the axial filament in its natural disposition inside its siliceous case.

In this article, a series of different approaches has been employed to investigate the inner structure of the axial filament, without altering its natural organization, to highlight some important features of the biosilicification process.

The presence of organic matter in some, but not all, microscleres has been reported (Garrone et al., 1981), but all our experiments (TGA, DSC, FTIR, and x-ray diffraction) on the analyzed microsclere samples did not reveal its presence.

From a phylogenetic point of view the main result of this research is the difference between the three species of demosponges and the hexactinellid *S. joubini*. The thermal analyses indicate that spicules from this last species have a greater percent of organic matter (15%) with respect to those from demosponges (~10%) and that the protein units in the axial filaments of these spicules are less closely packed. This is confirmed by the fiber diffraction experiments, which show that the distance between the repeating units of the highly ordered hexagonal patterns forming the filaments is greater in *S. joubini* spicules (8.4 nm) than in those of the three considered demosponges (5.8 nm) (Fig. 6).

These three species of demosponges are phylogenetically very far and belong to different orders: Tetractinellida, Hadromerida, and Haplosclerida. The similarity of the structural features of their axial filaments indicates an ancient basic origin of the process of spicule secretion, probably common to all demosponges.

Despite this homogeneity, the DSC and the fiber diffraction analyses revealed significant differences in the endothermal dehydration and/or protein unfolding processes and in the degree of order within the spicule filaments. The understanding of these differences needs further investigations, to highlight in particular the role played by the thickness of the siliceous cage in determining the nature of the modifications induced in the protein filament by thermal treatments under controlled conditions.

Our preliminary fiber diffraction results on *T. aurentium* oxeas are quite different from the interpretation of the x-ray diffraction diagrams of the extracted filaments given by Shimizu et al. (1998); indeed in the rather complex fiber pattern (Fig. 5 *a*) there is no evidence of a 17.2-nm periodicity. As already mentioned the difference might be ascribed to the effects of the rather aggressive extraction procedure. The novel use of the fiber diffraction technique, together with synchrotron radiation, for the structural study of spicules has allowed the analysis of the axial filaments inside their natural siliceous case. The mentioned hypothesis, suggested by our diffraction results (Croce et al., 2003), that silica contributes to the formation of the highly ordered arrangement of protein units in the axial filament by embodying the units in a regular mesoporous scaffolding, would also explain the dramatic effects of filament extraction by chemical methods.

The FTIR analysis has clearly indicated that the protein molecules in the axial filament interact via hydrogen bonds with the Si-OH groups of the inorganic matrix. Furthermore, the structural match between silicateins and cathepsin L has been further proved by the evidences on the prevalence of β-sheet structures in the analyzed spicule proteins.

Finally, the structural study was complemented by the theoretical calculations to shed some light, at a detailed molecular level, on the role of silicatein in the biosilicification process. From the molecular simulations we have obtained some preliminary hints about the role of the spicule proteins in promoting the process of silica polymerization. Indeed, the simulation of the interactions between the silicatein active site and orthosilicic acid or its deprotonated anion has shown that the rotation of the serine and histidine side chains, through the formation of hydrogen bonds, can bring two orthosilicic acid units together, and that the formation of a $(OH)_3$Si-O-Si$(OH)_3$ dimer is an energetically favored process.

All these data should be helpful for the disclosure of the detailed mechanisms of silica deposition and of spicule organization in sponges. This matter is relevant not only for the complex and not yet completely clarified phylogenesis of sponges based on spicule shape analysis but also for the important biotechnological approaches arising from the exploitation of recombinant silicateins for the construction of controlled silica nanostructures (Morse et al., 2000; Muller et al., 2002).

REFERENCES

Amenitsch, H., M. Rappolt, M. Kriechbaum, H. Mio, P. Laggner, and S. Bernstorff. 1998. First performance assessment of the small angle X-ray scattering beamline at ELETTRA. *J. Synchrotron Radiat.* 5:506–508.

Bendz, G., and I. Lindqvist, editors. 1977. Biochemistry of Silicon and Related Problems. Plenum Press, New York.

Berman, H. M., J. Westbrook, Z. Feng, G. Gilliland, T. N. Bhat, H. Weissig, I. N. Shindyalov, and P. E. Bourne. 2000. The Protein Data Bank. *Nucleic Acids Res.* 28:235–242.

Berti, P. J., and A. C. Storer. 1995. Alignment/phylogeny of the papain superfamily of cysteine proteases. *J. Mol. Biol.* 246:273–283.

Burneau, A., and J. P. Gallas. 1998. The Surface Properties of Silicas. A. P. Legrand, editor. John Wiley and Sons, Chichester, UK.

Cha, J. N., K. Shimizu, Y. Zhou, S. C. Christiansen, F. Bradley, G. D. Stucky, and D. E. Morse. 1999. Silicatein filaments and subunits from a marine sponge direct the polymerization of silica and silicones in vitro. *Proc. Natl. Acad. Sci. USA.* 96:361–365.

Cha, J. N., G. D. Stucky, D. E. Morse, and T. J. Deming. 2000. Biomimetic synthesis of ordered silica structures mediated by block copolypeptides. *Nature.* 403:289–292.

Cornell, W. D., P. Cieplak, C. I. Bayly, I. R. Gould, K. M. Merz, Jr., D. M. Ferguson, D. C. Spellmeyer, T. Fox, J. W. Caldwell, and P. A. Kollman. 1995. A second generation force field for the simulation of proteins, nucleic acids, and organic molecules. *J. Am. Chem. Soc.* 117:5179–5197.

Croce, G., A. Frache, M. Milanesio, D. Viterbo, G. Bavestrello, U. Benatti, M. Giovine, and H. Amenitsch. 2003. SAXS study of spicules from marine sponges. *Microsc. Res. Tech.* 62:378–381.

Custodio, M. R., E. Hajdu, and G. Muricy. 2002. In vivo study of microsclere formation in sponges of the genus Mycale (Demospongiae, Poecilosclerida). *Zoomorphology.* 121:203–211.

De Vos, L., K. Rutzler, N. Boury-Esnault, and J. Vacelet, editors. 1991. Atlas of Sponge Morphology. Smithsonian Institute, Washington, DC.

Frisch, M. J., G. W. Trucks, H. B. Schlegel, G. E. Scuseria, M. A. Robb, J. R. Cheeseman, V. G. Zakrzewski, and J. A. Montgomery. Jr., R. E. Stratmann, J. C. Burant, S. Dapprich, J. M. Millam, A. D. Daniels, K. N. Kudin, M. C. Strain, O. Farkas, J. Tomasi, V. Barone, M. Cossi, R. Cammi, B. Mennucci, C. Pomelli, C. Adamo, S. Clifford, J. Ochterski, G. A. Petersson, P. Y. Ayala, Q. Cui, K. Morokuma, D. K. Malick, A. D. Rabuck, K. Raghavachari, J. B. Foresman, J. Cioslowski, J. V. Ortiz, A. G. Baboul, B. B. Stefanov, G. Liu, A. Liashenko, P. Piskorz, I. Komaromi, R. Gomperts, R. L. Martin, D. J. Fox, T. Keith, M. A. Al-Laham, C. Y. Peng, A. Nanayakkara, C. Gonzalez, M. Challacombe, P. M. W. Gill, B. G. Johnson, W. Chen, W. M. Wong, J. L. Andres, M. Head-Gordon, E. S. Replogle, and J. A. Pople. 1998. GAUSSIAN 98 (Revision A.7). Gaussian, Inc., Pittsburgh, PA.

Garrone, R. 1978. Phylogenesis of Connective Tissue. Karger, Basel.

Garrone, R., T. L. Simpson, and J. Pottu-Boumendil. 1981. Ultrastructure and depisition of silica in sponges. *In* Silicon and Siliceous Structure in Biological Systems. T. L. Simpson and B. E. Volcani, editors. Springer, New York. 495–525.

Grosso, D., F. Babonneau, M. Klotz, P.-A. Albouy, H. Amenitsch, A. R. Balkenende, A. Brunet-Bruneau, and J. Rivory. 2002. An in situ study of mesostructured CYAB-silica film formation during dip coating using time-resolved SAXS and interferometry measurements. *Chem. Mater.* 14:931–939.

Guncar, G., G. Pungercic, I. Klemencic, V. Turk, and D. Turk. 1999. Crystal structure of MHC class II-associated p41 Ii fragment bound to cathepsin L reveals the structural basis for differentiation between cathepsins L and S. *EMBO J.* 18:793–803.

Hammersley, A. P. 1995. ESRF Internal Report, EXP/AH/95–01, FIT2D V5.18 Reference Manual V1.6. Grenoble, France.

Hammersley, A. P., S. O. Svensson, M. Hanfland, A. N. Fitch, and D. Häusermann. 1996. Two-dimensional detector software: from real detector to idealised image or two-theta scan. *High Pressure Res.* 14:235–248.

Haris, P. I., and F. Severcan. 1999. FTIR spectroscopic characterization of protein structure in aqueous and non-aqueous media. *J. Mol. Catal. B Enzym.* 7:207–221.

Hooper, J. N. A., and W. M. Van Soest, editors. 2003. Systema Porifera: A Guide to the Classification of Sponges. Plenum Pub. Corp., New York.

Krasko, A., V. Gamulin, J. Seack, R. Steffen, H. C. Schröder, and W. E. G. Müller. 1997. Cathepsin, a major protease of the marine sponge Geodia cydonium: purification of the enzyme and molecular cloning of cDNA. *Mol. Mar. Biol. Biotechnol.* 6:296–307.

Krasko, A., B. Lorenz, R. Batel, H. C. Schroder, I. M. Muller, and W. E. Muller. 2000. Expression of silicatein and collagen genes in the marine sponge Suberites domuncula is controlled by silicate and myotrophin. *Eur. J. Biochem.* 267:4878–4887.

Mann, S. 2001. Biomineralization. Oxford University Press, Oxford, UK.

Morse, D. E., G. D. Stuckey, T. D. Deming, J. Cha, K. Shimuzu, and Y. Zhou. 2000. Methods, Compositions, and Biomimetic Catalysts for in Vitro Synthesis of Silica, Polysilsequioxane, Polysiloxane, and Polymetallo-Oxanes. Worldwide Patent WO 00/35993 A1.

Muller, W. E. G., H. C. Schroder, B. Lorenz, and A. Krasko. 2002. Silicatein-Mediated Synthesis of Amorphous Silicates and Siloxanes and Use Thereof. Worldwide Patent WO 02/10420 A2.

Murakami, K. 2002. The National Center for Biotechnology Information (NCBI) accession number BAB86343.

Perry, C. C., and T. Keeling-Tucker. 2000. Biosilicification: the role of organic matrix in structure control. *J. Biol. Inorg. Chem.* 5:537–550.

Shimizu, K., J. Cha, G. D. Stucky, and D. E. Morse. 1998. Silicatein α: cathepsin L-like protein in sponge biosilica. *Proc. Natl. Acad. Sci. USA.* 95:6234–6238.

Simpson, T. L. 1984. The Cell Biology of Sponges. Springer, New York.

Simpson, T. L., and B. E. Volcani, editors. 1981. Silicon and Siliceous Structures in Biological Systems. Springer, New York.

Ugliengo, P., D. Viterbo, and G. Chiari. 1993. MOLDRAW: molecular graphics on a personal computer. *Z. Krist.* 207:9–23. (http://www.ch.unito.it/ifm/fisica/moldraw/moldraw.html).

Uriz, M. J., X. Turon, and M. A. Becerro. 2000. Silica deposition in Demosponges: spiculogenesis in Crambe crambe. *Cell Tissue Res.* 301:299–309.

Voronkov, M. G., G. I. Zelchan, and E. J. Lukevits. 1977. Silicon and Life, 2nd ed. Zinatne, Riga, Latvia.

Zhou, Y., K. Shimizu, J. Cha, G. D. Stucky, and D. E. Morse. 1999. Efficient cayalysis of polysiloxane synthesis by silicatein α requires specific hydroxy and imidazole functionalities. *Angew. Chem. Int. Ed.* 38:779–782.